J. Biomechanics Vol. 19, No. 12, pp. 1015–1022, 1986.
Printed in Great Britain

0021–9290/86 $3.00 + .00
Pergamon Journals Ltd.

A GLOBAL MATHEMATICAL MODEL OF THE CEREBRAL CIRCULATION IN MAN

MOKHTAR ZAGZOULE*† and JEAN-PIERRE MARC-VERGNES†

*Laboratoire de Mécaniqué, Groupe de rhéologie, Université Paul Sabatier, 118 route de Narbonne, 31062 Toulouse Cedex, France; †LHEC-INSERM U.230, Chu Purpan, 31059 Toulouse Cedex, France

Abstract—A mathematical model of the cerebral circulation has been formulated. It was based on non-linear equations of pulsatile fluid flow in distensible conduits and applied to a network simulating the entire cerebral vasculature, from the carotid and vertebral arteries to the sinuses and the jugular veins. The quasi-linear hyperbolic system of equations was numerically solved using the two-step Lax–Wendroff scheme. The model's results were in good agreement with pressure and flow data recorded in humans during rest. The model was also applied to the study of autoregulation during arterial hypotension. A close relationship between cerebral blood flow (CBF) and capillary pressure was obtained. At arterial pressure of 80 mmHg, the vasodilation of the pial arteries was unable to maintain CBF at its control value. At the lower limit of autoregulation (60 mm Hg), CBF was maintained with a 25% increase of zero transmural pressure diameter of nearly the whole arterial network.

INTRODUCTION

How does the vascular cerebral network determine the cerebral circulation at a physiological state of rest? How does its vasomotor activity modulate the adaptative hemodynamic changes in response to physiological stimulations? Experimental studies cannot fully answer these two questions since only the behavior of the pial network can be directly observed. Also, it is difficult to simultaneously measure cerebral blood flow (CBF) and vessel diameter changes in man. A mathematical model in which all the parameters can be controlled, may be a valuable tool for a better understanding of this particular vascular system.

The previous mathematical modelling of the cerebral circulation has been focused on the circle of Willis and its afferent and efferent vessels. Since its first description by Willis in 1664, this very peculiar arterial structure has been considered either as an equalizing system for pressure and flow, or as an anastomotic system which only functions in pathological conditions. These two hypotheses have given rise to several models (Rogers, 1947; Avmann and Bering, 1961; Murray, 1964; Himwich *et al.*, 1965; Himwich and Clark, 1971; Clark *et al.*, 1967, 1968; Chao and Hwang, 1971; Kufahl *et al.*, 1981; Hillen *et al.*, 1982).

However, the circle of Willis is only a limited part of the cerebral vasculature. The pial network, the intracerebral arteries, the microcirculation and the venous network, also play an important role in the regulatory process of cerebral hemodynamics.

Thus, our objective was to elaborate a mathematical model based on fluid mechanic concepts including pulsatile flow in elastic tubes and applied to a network simulating the entire cerebral vasculature. We present here the first version of this model with an application to the study of autoregulation, i.e. the ability of the cerebral vascular network to maintain a constant cerebral blood flow in spite of a wide range of perfusion pressures.

Received 26 *July* 1985; *in revised form* 6 *May* 1986.

METHODS

Morphological and rheological data

The simplified morphological scheme that we propose reproduces the major features of the cerebral vasculature and is shown in Fig. 1. It begins at the origin of the internal carotid [1 and 2 on Fig. 1] and vertebral [3 and 4] arteries. All of the important vessels are represented individually: the fusion of the vertebral arteries into the basilar artery [5, 6], the arteries forming the circle of Willis [7–14], the middle [17, 18] and posterior [15, 16] cerebral arteries. The only exceptions are the two anterior cerebral arteries which are replaced by a single vessel [19]. The vessel emerging between [5] and [6] is a peripheral resistance representing the brainstem and the cerebellar vascular network. The rest of the arterial system is grouped into three successive tubes, each one representing a characteristic part of the arterial network: the principal collaterals of the cerebral arteries [20], the pial network [21] and the intracerebral arteries [22]. The microcirculation, including the terminal arterioles, the pre-capillaries, the capillaries and the venulas, is represented by one tube [23]. The tubes 24 and 25 simulate a part of the network corresponding, respectively, to intracerebral and pial veins. The following segments represent the groups of veins which drain directly into

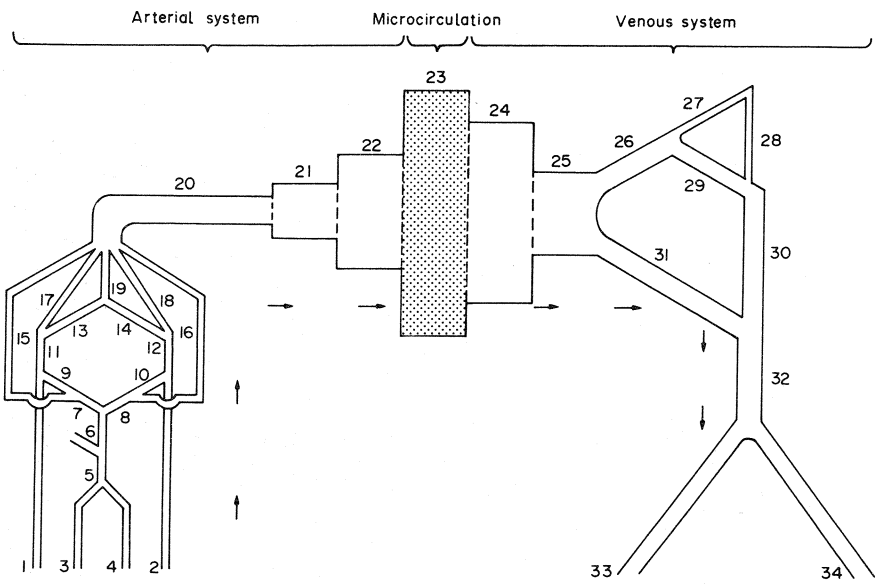

Fig. 1. Schematic diagram of the cerebral vasculature. The numbers refer to the arteries and veins as listed in Table 1.

the sinuses [28, 30, 32], they themselves merging into the jugular veins [33, 34].

The data, concerning lengths, cross-sections and the number of vessels, were taken from the literature when they were available (Lazorthes, 1961; Lazorthes *et al.*, 1976, 1979; Blinkov and Glezer, 1969; Van der Eecken, 1959; Hunziker and Schweizer, 1977; Hunziker *et al.*, 1978, 1979; Parmaret, 1958). In order to determine the lengths, the cross-sectional areas and the number of vessels for which no data are available, we assumed a geometric progression between the cerebral arteries and the microcirculation. This progression was done in such a way that we obtained a capillary pressure of about 25 mmHg for the diastolic flow. The same approach was used for the venous system.

The rheological data used for the vessel walls were taken from Moritake *et al.* (1974), Moritake (1975), Nagasawa *et al.* (1979), Hayashi *et al.* (1980), and Hudetz *et al.* (1981). However, these authors only considered the major afferent vessels. For the rheological data that was lacking, we used a global relation based on the increasing rigidity of the arteries from the heart to the periphery (Anliker *et al.*, 1971). For the venous system, an inverse relation, i.e. a decreasing rigidity towards larger veins, was assumed except for the sinuses which were considered as quasi-rigid. All the morphometrical and rheological data necessary for the computation are given in Table 1.

Mathematical formulation

The blood was considered as a viscous and incompressible fluid that flows through distensible tubes of circular cross-section. Since the pressure wave length was long compared to the vessel diameter, the blood flow was considered to be unidimensional. The equations governing the blood flow coupled with vessel wall movement are as follows

continuity
$$\frac{\partial A}{\partial t}+\frac{\partial (AU)}{\partial x}=0 \tag{1}$$

momentum
$$\frac{\partial U}{\partial t}+\frac{\partial}{\partial x}\left(\frac{U^2}{2}+\frac{P}{\rho}\right)=-F \tag{2}$$

tube law
$$P=E_L\left(\frac{A}{A_0}-1\right) \tag{3}$$

where
$$E_L=\frac{E}{2}\frac{h}{R_0}$$

U being the average fluid velocity over the cross-section A, P the transmural pressure, ρ the fluid density, F the friction term which accounts for viscous drag between the blood and the vessel wall, E Young's modulus, and h the wall thickness. A_0 and R_0 represent, respectively, the cross-section and the radius at zero transmural pressure.

For the laminar flow, the friction term (F) was expressed in terms of true vessel cross-sectional area as

$$F=\frac{8\pi\mu}{\rho}\frac{U}{A}=\gamma\frac{U}{A}$$

μ being the dynamic viscosity coefficient.

When N such vessels were combined to form an equivalent tube, this friction term was expressed in terms of the total cross-section S ($S = NA$) as follows (Collins and Maccario, 1979)

$$F=N\frac{8\pi\mu}{\rho}\frac{U}{S}.$$

For small values of the Womersley dimensionless parameter (α), the Poiseuille term (F) which, theoreti-

Table 1. Morphological and rheological data used in the model

Segment number(s)	Vessels	Cross-section A_0 (cm^2)	Length L (cm)	Elastance E_L (10^5 dyn cm^{-2})	Number of vessels
1 and 2	Internal carotid arteries (below posterior communicating arteries)	0.14	25.0	13.67	1
3 and 4	Vertebral arteries	0.09	25.0	13.67	1
5	Basilar artery: first part	0.19	2.0	27.35	1
6	Basilar artery: second part	0.09	2.0	27.35	1
7 and 8	Posterior cerebral arteries	0.07	2.0	27.35	1
9 and 10	Posterior communicating arteries	0.02	2.0	27.35	1
11 and 12	Internal carotid arteries (above posterior communicating arteries)	0.14	2.0	27.35	1
13 and 14	Anterior cerebral arteries (below anterior communicating arteries)	0.07	2.0	27.35	1
15 and 16	Posterior cerebral arteries	0.07	25.0	30.08	1
17 and 18	Middle cerebral arteries	0.12	35.0	30.08	1
19	Anterior cerebral arteries (above posterior communicating arteries)	0.12	25.0	30.08	2
20	Main branches of cerebral arteries	0.55	10.0	33.09	50
21	Pial network	1.75	3.5	36.40	3900
22	Intracerebral arteries	4.74	3.5	40.04	35000
23	Microcirculation	38.0	0.5	44.04	202000
24	Intracerebral veins	9.49	3.5	27.35	72000
25	Pial veins	3.86	3.5	13.0	3800
26	Cerebral veins	0.92	5.0	5.17	40
27	Cerebral veins	0.33	5.0	5.0	10
28	Longitudinal sinuses: first part	0.15	15.0	117.0	2
29	Veins	0.49	15.0	5.0	10
30	Longitudinal sinuses: second part	0.47	20.0	117.25	2
31	Veins	0.29	10.0	5.0	30
32	Transverse sinuses	1.65	5.0	117.78	1
33 and 34	Jugular veins	0.43	15.0	2.65	1

cally, is only valid for steady flow can be used as a first approximation and is widely applied in hemodynamic studies. In our model, the largest value of α is about five for the internal carotid artery which has negligible resistance relative to the whole network.

Equation (3) expresses the relation between the transmural pressure and the cross-sectional area. This linear relation is purely elastic.

Equations (1), (2) and (3) form a first-order quasi-linear hyperbolic system. The numerical resolution method used here is the two-step Lax–Wendroff scheme (Richtmeyer and Morton, 1967; Kivity and Collins, 1974)

step I

$$\left.\begin{aligned} A_{j+1/2}^{n+1/2} &= \frac{A_j^n + A_{j+1}^n}{2} - \frac{\Delta t}{2\Delta x}(A_{j+1}^n U_{j+1}^n - A_j^n U_j^n) \\ U_{j+1/2}^{n+1/2} &= \frac{U_j^n + U_{j+1}^n}{2} - \frac{\Delta t}{2\Delta x}\left[\left(\frac{U^2}{2}+\frac{P}{\rho}\right)_{j+1}^{n} - \left(\frac{U^2}{2}+\frac{P}{\rho}\right)_{j}^{n}\right] - \frac{\Delta t}{2} F_{j+1/2}^n \\ \text{where} \quad F_{j+1/2}^n &= \frac{8\pi\mu}{\rho} n \left(\frac{U_{j+1}^n}{A_{j+1}^n} + \frac{U_j^n}{A_j^n}\right)\Big/ 2 \\ P_{j+1/2}^{n+1/2} &= E_L\left(\frac{A_{j+1/2}^{n+1/2} - A_{0j}}{A_{0j}}\right) \end{aligned}\right\} \quad (4)$$

step II

$$\left.\begin{aligned} A_j^{n+1} &= A_j^n - \frac{\Delta t}{\Delta x}\left((AU)_{j+1/2}^{n+1/2} - (AU)_{j-1/2}^{n+1/2}\right) \\ U_j^{n+1} &= U_j^n - \frac{\Delta t}{\Delta x}\left[\left(\frac{U^2}{2}+\frac{P}{\rho}\right)_{j+1/2}^{n+1/2} - \left(\frac{U^2}{2}+\frac{P}{\rho}\right)_{j-1/2}^{n+1/2}\right] - \Delta T F_j^{n+1/2} \\ \text{where} \quad F_j^{n+1} &= \frac{8\pi\mu}{\rho} n \left[\left(\frac{U}{A}\right)_{j+1/2}^{n+1/2} + \left(\frac{U}{A}\right)_{j-1/2}^{n+1/2}\right]\Big/ 2 \\ P_j^{n+1} &= E_L(A_j^{n+1}/A_{0j} - 1). \end{aligned}\right\} \quad (5)$$

The j subscripts indicate intervals in distance x along a tube, while the n superscripts denote the time interval.

We used as boundary conditions either P at proximal end and U at distal end of the network, or P at both network extremities. In both cases, the same results were obtained. The additional numerical boundary conditions required for the finite difference equations were determined by uncentered approximations (Warming *et al.*, 1983). For instance, in the case where P was given at the proximal end, U was

evaluated at the entry by the following scheme

$$U_0^{n+1} = U_0^n - \frac{\Delta t}{\Delta x}\left[\left(\frac{U^2}{2}+\frac{P}{\rho}\right)_1^n - \left(\frac{U^2}{2}+\frac{P}{\rho}\right)_0^n\right] - \Delta t F_0^n$$

which is an uncentered approximation of the momentum equation between 0 and 1. 0 denotes the entry and 1 is the point just ΔX distant from it.

In order to determine the internal boundary conditions at bifurcations, the following relations were used

$$(AU)_{j,1} = (AU)_{0,2} + (AU)_{0,3} \tag{6}$$

$$P_{j,1} = P_{0,2} = P_{0,3} \tag{7}$$

where subscripts 0 and j denote, respectively, the beginning and the end of a segment, 1 being the parent branch, 2 and 3 denoting the daughter branches. Each section A is related to the pressure through the segment corresponding tube law, i.e. equation (3) in which E_L may be different for each branch of the bifurcation. Three equations relating section to pressure are thus obtained.

As we have nine unknowns, the three remaining equations were obtained by approximating the continuity equation at the point $j-1$ of the parent tube and $0+1$ of the daughter tubes with the following scheme

$$\left[\frac{\frac{A_j^{n+1}+A_{j-1}^{n+1}}{2} - \frac{A_j^n + A_{j-1}^n}{2}}{\Delta t} + \frac{(AU)_j^{n+1} - (AU)_{j-1}^{n+1}}{\Delta X}\right]_1 = 0 \tag{8}$$

$$\left[\frac{\frac{A_1^{n+1}+A_0^{n+1}}{2} - \frac{A_1^n + A_0^n}{2}}{\Delta t} + \frac{(AU)_1^{n+1} - (AU)_0^{n+1}}{\Delta X}\right]_i = 0. \tag{9}$$

At junctions between two segments of different cross-sectional area, as between (20) and (21), the system reduces to six equations instead of nine, while at the confluence of the five efferent vessels into segment (20) we have eighteen equations.

The system is integrated in a step-wise marching procedure in time. The initial conditions of a permanent flow with estimated diastolic values are used to evaluate the right-hand sides of equation (4), from which one obtains the new values of A, U and P at the next half time step for each position x. These values in turn are used to evaluate the right-hand sides of (5), which then yield the values of A, U and P advanced to the full time step. Internal boundaries are calculated using the relations (6)–(9). With the given and the calculated external boundary conditions, one returns to the first step and continues in time.

Since the transmural pressure depends solely upon the local cross-section and not upon its derivatives, the hyperbolic stability criterion is therefore (Richtmeyer and Morton, 1967)

$$\left|(|U|+C)\frac{\Delta t}{\Delta x}\right| \leqslant 1$$

where C is the pressure wave velocity. This criterion also assures the stability of the uncentered approximations that were used to complete the boundary conditions (Gottlieb, 1978).

Satisfying this stability condition in a network which is composed of tubes possessing different lengths and wave velocities implies advancing by different time increments. Interpolation procedures were then applied in order to match the 'slower' wave speed zones with the 'rapid' ones (Zagzoule, 1983).

The input pressure, depicted in Fig. 2, was taken from Remington (1963), where it is given as the pressure signal in the subclavian artery, and applied simultaneously to all four inputs. The output pressure at the jugular veins is taken to be constant and equal to 5 mm Hg. Starting computation with a permanent flow with estimated diastolic value, the periodicity is reached in the second cycle.

RESULTS

Baseline values

The numerical results of the model for the standard case, corresponding to a physiological state of rest, are represented by computer drawn graphs, which give the computed velocities (Fig. 3) and pressures (Fig. 4) at the entrance of some segments of the network. From these numerical results, we deduced flow and pressure values averaged over one cardiac cycle.

The global cerebral blood flow calculated by the model equalled 12.8 $cm^3\,s^{-1}$, which corresponds to 55 ml 100 g^{-1} min^{-1}. This value is very close to that of 54 ml 100 g^{-1} min^{-1} found by Kety and Schmidt (1948) and confirmed by many other authors (for review, see Lassen, 1959, and Harper, 1969). Flow distribution in the afferent and efferent vessels of the circle of Willis is given in Table 2.

Figure 5 shows the model's predictions for the location of pressure drop in the cerebral vascular network. As for the instantaneous values, the shape of the curves measuring the velocity at the proximal and distal boundaries of the model are in good agreement with those recorded by Doppler velocimetry at the carotid artery and at the jugular vein.

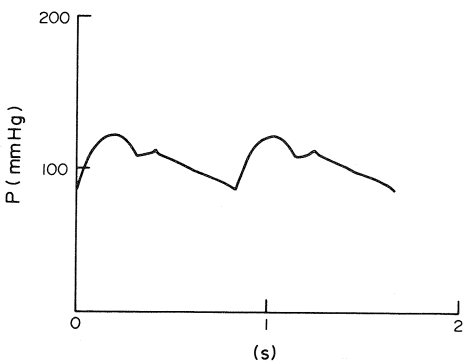

Fig. 2. The pressure signal at the entrance of the model.

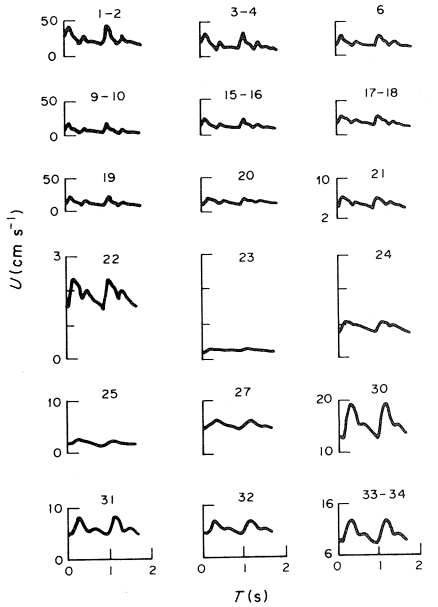

Fig. 3. The computed velocity signals at different locations of the cerebral vasulature. The numbers refer to the arteries and veins as listed in Table 1.

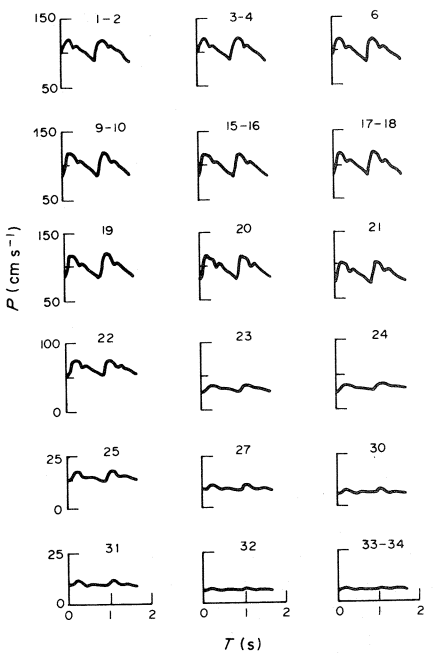

Fig. 4. The computed pressure signals at different locations of the cerebral vasculature. The numbers refer to the arteries and veins as listed in Table 1.

Autoregulation

An important feature of the cerebral circulation is the phenomenon of autoregulation. It is well established that, in spite of a wide range of blood pressures, the cerebral blood flow remains constant (for review, see Lassen, 1959). This constancy implies,

Table 2. Blood flow distribution in afferent and efferent vessels of the circle of Willis as predicted by the model compared to measured data

	Kristiansen and Krog (1962)	Austin (1970)	Model
	(Percent of CBF)		
Internal carotid artery	75.3	72.6	68.2
Vertebral artery	24.7	27.4	31.8
Middle cerebral artery	—	62	57.7
Posterior cerebral artery	—	20	22.2
Anterior cerebral artery	—	18	20.2

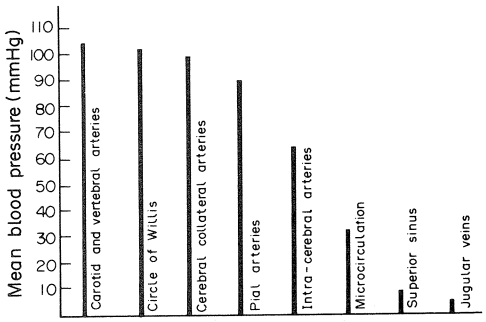

Fig. 5. Mean pressure values at different locations of the cerebral network as predicted by the model.

as it has been experimentally verified, vasodilation as blood pressure falls (Fog, 1937) and vasoconstriction as the blood pressure rises (Fog, 1939).

We chose this phenomenon as a first application of the model. We did not try to simulate the autoregulation process as it effectively occurs in the cerebral circulation. We only simulated the changes in the caliber of the vessels, independently of the mechanism responsible of these changes. Several numerical tests were performed by lowering the mean arterial blood pressure at the proximal end of the model and by increasing the zero transmural pressure diameters ($D\emptyset$) in the arterial parts of the network. A step by step change in blood pressure was used: 105, 90, 80, 60 and 40 mm Hg. For each blood pressure value, a 25%, 50%, 75% and 100% $D\emptyset$ increase was applied to the whole network and to the different parts of it. When no $D\emptyset$ change was carried out, a linear relationship between flow and perfusion pressure was obviously obtained. Furthermore, as can be seen in Fig. 6, in all cases a very close linear relationship was observed between CBF and the capillary pressure. Figure 6 shows the results obtained by only modifying the $D\emptyset$ of segment [21] (pial network), but similar results were observed with the other segments. In each case, CBF remained at its control value as long as the capillary pressure was maintained at its own control level, i.e., 32 mm Hg.

The $D\emptyset$ changes between 0 and 25% were the most effective in compensating CBF decrease during hypo-

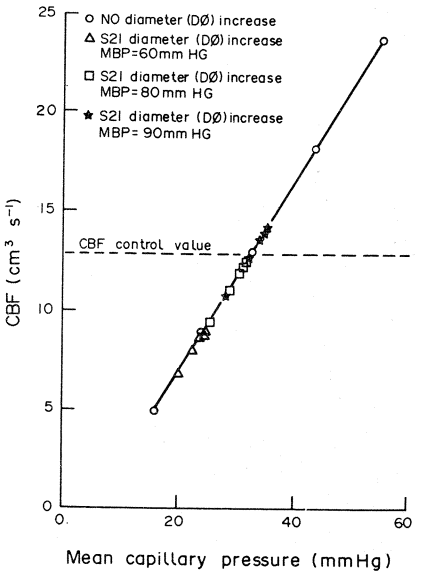

Fig. 6. The effects on CBF of zero transmural pressure diameter ($D\emptyset$) increase of segment [21] (pial arteries) at different mean blood pressure (M.B.P.).

tension. This result was true to a lesser extent in the 25–50% range. Beyond this last value, the effect of $D\emptyset$ changes were negligible. This observation was true for all the pressures considered. This result confirms the experimental findings of Kontos *et al.* (1978) and Mackenzie *et al.* (1979) who observed that pial arteries continued to dilate below the lower limit of autoregulation without effect on the regulation of CBF. Figure 7 shows the results obtained with the segment (21), 'the pial arteries'. It can also be seen that, at a perfusion pressure of 80 mm Hg, the pial artery vasodilation in itself was not sufficient to maintain CBF at its control value. Similar results were obtained with segment (22), 'intracerebral arteries', whereas the other parts of the arterial network were clearly less effective. At the 'lower limit of autoregulation' which corresponds to a perfusion pressure of 60 mm Hg, a simultaneous $D\emptyset$ increase of about 50% in both pial and intracerebral arteries was necessary to maintain a CBF value of 12.8 $cm^3 s^{-1}$ (55 ml $100 g^{-1} min^{-1}$). The same result was achieved by a simultaneous $D\emptyset$ increase of only 25% in segments [20, 21, 22].

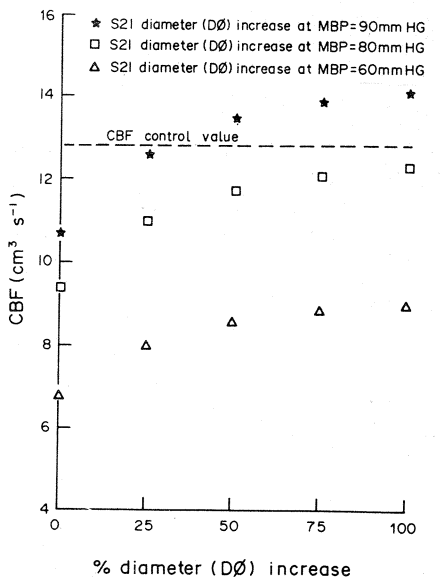

Fig. 7. Relationship between the CBF and mean capillary pressure obtained by the model for different mean blood pressures (M.B.P.) and various vasodilation levels of segment [21] (pial arteries).

DISCUSSION

Our model used simplifications. First, by regrouping the principal collaterals of the cerebral arteries and the pial network into equivalent tubes, we cannot evaluate the compensating rôle of cortical anastomoses which connect cerebral arteries at the limit of their territories, nor can we evaluate the relative rôle of different cerebral regions in autoregulation. However, these evaluations were not the aim of this study. The global behaviour of this network, as far as autoregulation is concerned, is not affected by this regrouping which was effected in order to reduce the computation time. The cerebral spinal fluid pressure was not taken into account either. Although its influence is negligible in normal physiological conditions (Betz, 1972; Ruch and Patton, 1974), it must be integrated into the model before studying the effects of posture and gravity. Finally, a rather rough morphometrical and rheological approach was used for modelling the microcirculation. A specific study of this part of the cerebral network is obviously needed.

Despite these simplifications, we were able to reach the objective of this work which was to formulate a global mathematical model of the cerebral circulation in order to study the blood flow/vasomotricity relationship. The first condition that the model was expected to fulfill was that it should provide results similar to the well-known hemodynamic values of the cerebral circulation while only giving the pressure as boundary conditions. This requirement was effectively met for the global cerebral blood flow and its distribution in the afferent and efferent vessels of the circle of Willis. As shown in Table 2, flow distribution was quite similar to that found experimentally (Kristiansen and Krog, 1962; Austin *et al.*, 1970).

With regard to pressure drop, Espagno *et al.* (1969) found an average pressure of 76 mm Hg in the submillimetric cortical arteries and 34 mm Hg in the microcirculation in man. These values and the ones given by the model are very close. Pressure drop has also been measured in animals, but with some discordances. Söderburg and Weckmann (1959) found in the cat that the pressure in the basilar artery was only about 10–30% of the systemic pressure, while Kanzow

and Dieckoff (1969) recorded that 42% of the total resistance occurred in the vessels that lead from the aorta to the pial arteries. This last result is in good agreement with the model's which predicts 41.5% of the total head loss in the corresponding part of our network.

Three main hypotheses have been proposed to explain the so-called 'autoregulation of the cerebral circulation': myogenic, metabolic and nervous. But, whatever factors are involved, the CBF is, at a given pressure gradient, mechanically regulated by changes in vascular smooth muscles which directly act on cross-sectional area and rheological properties of the vessels. However the effects of these mechanical parameters on CBF, even though of great importance, have not been very closely studied. The vascular smooth muscle tone can vary the cross-sectional area, the thickness-to-radius ratio, the parietal elasticity, and very likely all of these parameters simultaneously. In this first approach, we did not try to simulate this complex action in detail but simply acted on the zero-transmural pressure diameter ($D\emptyset$). However, these modifications were sufficient to show the arterial network's ability to maintain autoregulation over a range of experimentally observed cross-sectional variations. It is noteworthy that, at the lower limit of autoregulation, the model gave the CBF control value by using the most effective range of vasodilation (25%) of almost the whole arterial network, without capillary or venous vasodilation. Furthermore, at mean arterial pressures below 60 mm Hg, the model showed that cerebral blood flow fell although cerebral arteries and arterioles continued to dilate. This result was in agreement with the experimental findings of Kontos *et al.* (1978) and Mackenzie *et al.* (1979). It has been experimentally shown by the same authors that the pial vessel responses during hypotension were size dependent. This point cannot be studied by the model as long as the pial arteries are grouped in a single tube. However, we found that pial and intracerebral arteries, which are the most resistive vessels, were also the most effective in maintaining CBF autoregulation, but with a quite similar effect as suggested by Kontos *et al.* (1979) and by Tuor and Farrar (1984).

Finally, we noticed that in our model the autoregulation was not limited to maintaining a global cerebral blood flow but also preserved the same blood flow distribution in afferent and efferent arteries of the circle of Willis, as well as a stable capillary pressure. So the question arises as to what parameter is regulated: CBF or capillary pressure?

In the light of these first results, we believe that our model can be considered as a realistic simulation of the cerebral circulation and as a valuable tool for studying its main concepts and features.

Acknowledgement—The authors would like to thank Dr Richard Collins for his valuable advice at the beginning of this work; Hamid Sahel, Gérard Viallard and Véronique Coelho for illustration; Phillip Link for translating the text; and Véronique Hermantier for typing the manuscript.

REFERENCES

Anliker, M., Rockwell, R. L. and Ogden, E. (1971) Non linear analysis of pulse waves and shock waves in arteries, *Z. angew. Math. Phys.* **22,** 217–246, 563–581.

Avmann, N. and Bering, E. A., Jr. (1961) A plastic model for the study of pressure changes in the circle of Willis and major arteries following arterial occlusion. *J. Neurosurg.* **18,** 361–365.

Austin, G., Horn, N. and Rouhe, S. (1970) Perfusion cerebral blood flow measured by argon inhalation and the mass spectrometer. *Brain and Blood Flow. Proceedings of the Fourth International Symposium on the Regulation of Cerebral Blood Flow* (Edited by Russel, R. W. R.), p. 22. Pitman, London.

Betz (1972) Cerebral blood flow: its measurement and regulation. *Physiol. Rev.* **52,** 595–630.

Blinkov, S. M. and Glezer, I. I. (1968) *The Human Brain in Figures and Tables.* Basic Books, New York.

Chao, J. C. and Hwang, N. H. C. (1971) A dynamic model of the circle of Willis. *J. Biomechanics* **4,** 141–147.

Clark, M. E., Himwich, W. A. and Martin, J. D. (1967) Simulation studies of factors influencing the cerebral circulation. *Acta. neurol. scand.* **43,** 189–204.

Clark, M. E., Himwich, W. A. and Martin, J. D. (1968) A comparative examination of cerebral circulation models. *J. Neurosurg.* **29,** 484–494.

Collins, R. and Maccario, J. A. (1979) Blood flow in the lung. *J. Biomechanics* **12,** 373–395.

Espagno, J., Arbus, L., Bes, A., Billet, R., Gouaze, A., Frerebeau, Ph., Lazorthes, Y., Salamon, G., Seylaz, J. and Vlahovitch, B. (1969) La circulation cérébrale. *Neuro-Chirurgie* **15,** Suppl. 2.

Fog, M. (1937) Cerebral circulation. The reaction of the pial arteries to a fall in blood pressure. *Archs Neurol. Psychiat., Chicago* **37,** 351–364.

Fog, M. (1939) Cerebral circulation: reaction of pial arteries to increase in blood pressure. *Archs Neurol. Psychiat., Chicago* **41,** 260–268.

Gottlieb, D. (1978) Boundary conditions for multistate P finite-difference methods for time-dependent equations. *J. Comput. Phys.* **26,** 181–195.

Harper, A. M. (1969) General physiology of cerebral circulation. *Cerebral Circulation* (Edited by Mac Dowall, D. G.). pp. 473–506. Little, Brown and Cowell, Boston.

Hayashi, K., Handa, H., Nagasawa, S., Okumura, A. and Moritake, K. (1980) Stiffness and elastic behavior of human intracranial extra-cranial arteries. *J. Biomechanics* **13,** 175–184.

Hillen, B., Gaasbeek, T. and Hoogstraten, W. (1982) A mathematical model of the flow in the posterior communicating arteries. *J. Biomechanics* **15,** 441–448.

Himwich, W. A., Knapp, F. M., Wenglarz, R. A., Martin, J. D. and Clark, M. E. (1965) The circle of Willis as simulated by an engineering model. *Archs Neurol., Chicago.* **13,** 164–172.

Himwich, W. A. and Clark, M. E. (1971) Cerebral blood flow comparisons between model and prototype. *J. appl. Physiol.* **31,** 873–879.

Hudetz, A. G., Mark, G., Kovach, A. G. B., Kerenyi, T., Fody, L. and Monos, E. (1981) Biomechanical properties of normal and fibrosclerotic human cerebral arteries. *Atherosclerosis* **39,** 353–365.

Hunziker, P. and Schweitzer, A. (1977) Postmortem changes in stereological parameters of cerebral capillaries. *Beitr. path. Anat.* **161,** 244–255.

Hunziker, P., Abdel'al, S., Shulz, U. and Schweitzer, A. (1978) Architecture of cerebral capillaries in aged human subjects with hypertension. *Adv. neurol.* **20,** 471–477.

Hunziker, P., Abdel'al, S. and Shulz, U. (1979) The aging human cortex: A stereological characterization of changes in the capillary net. *J. Geront.* **34,** 345–350.

Kanzow, E. and Dieckhoff, D. (1969) On the location of the vascular resistance in the cerebral circulation. *Cerebral*

Blood Flow (Edited by Brock, M., Fieschi, C., Ingvar, D. H., Lassen, N. A. and Shurmann, K.) pp. 96–97. Springer, Berlin.

Kety, S. S. and Schmidt, C. F. (1948) The nitrous oxydemethod for the quantitative determination of cerebral blood flow in man: theory, procedure and normal values. *J. clin. Invest.* **27,** 476–483.

Kivity, Y. and Collins, R. (1974) Nonlinear wave propagation in viscoelastic tubes: application to aortic rupture. *J. Biomechanics* **7,** 67–76.

Kontos, H. A., Enoch, P. W., Navari, R. M., Levasseur, J. E., Rosemblum, W. I. and Patterson, J. L., Jr. (1978) Responses of cerebral arteries and arterioles to acute hypotension and hypertension. *Am. J. Physiol.* **234,** H371–H383.

Kristiansen, K. and Krog, J. (1962) Electromagnetic studies on the blood flow through the carotid system in man. *Neurology, Minneap.* **12,** 20.

Kufahl, R. H., Horton, R. C., Hudetz, A. G. and Clark, M. E. (1981) A computer simulation of pulsatile cerebral blood flow. *Proceedings of the 34th Annual Conference on Engineering in Medicine and Biology.* Houston, Texas. Vol. 23, ACEMB Publishers.

Lassen, N. A. (1959) Cerebral blood flow and oxygen consumption in man. *Physiol. Rev.* **39,** 183–238.

Lazorthes, G. (1961) *Vascularisation artérielle cérébrale.* Masson et Cie, Paris.

Lazorthes, G., Gouaze, A. and Salamon, G. (1976) *Vascularisation et circulation de l'encéphale. T1: Anatomie descriptive et fonctionnelle.* Masson et Cie, Paris.

Lazorthes, G., Gouaze, A., Santini, J. J. and Salamon, G. (1979) Le cercle artériel du cerveau (circulus arteriosus cerebri). *Anat. clin.* **1,** 241–257.

Mackenzie, E., Farrar, J. K., Fitch, W., Graham, D. I., Gregory, P. C. and Harper, A. M. (1979) Effects of hemorrhagic hypotension on the cerebral circulation. I. Cerebral blood flow and pial arteriolar caliber. *Stroke,* **10,** 711–718.

Moritake, K., Handa, H., Okumura, A., Hayashi, K. and Niimi, H. (1974) Stiffness of cerebral arteries—its role in the pathogenesis of cerebral aneurysms. *Neurol. medico-chirurgica* **14,** I.

Moritake, K. (1975) Biomechanical studies on the pathogenisis of cerebral aneurysms and the mechanism of their growth and rupture. *Jap. Chir.* **44,** 87–107, 108–123.

Murray, K. (1964) Dimensions of the circle of Willis and dynamic studies using electrical analogy. *J. Neurosurg.* **21,** 26–34.

Nagasawa, S., Handa, H., Okumura, A., Naruo, Y., Moritake, K. and Hayashi, K. (1979) Mechanical properties of human cerebral arteries. Part I: Effects of age and vascular smooth muscle activation. *Surg. Neurol.* **12,** 297–304.

Paturet, G. (1958) *Traité d'anatomie humaine.* T. IV. Masson, Paris.

Purves, M. J. (1972) *The Physiology of the Cerebral Circulation.* Cambridge University Press, Cambridge.

Remington, J. W. (1963) The physiology of the aorta and major arteries. *Handbook of Physiology, section 2: Circulation* Vol. 2, (Edited by Hamilton, W. F. and Dow, P.), p. 799. American Society, Washington, DC.

Richtmeyer, R. D. and Morton, K. W. (1967) *Difference Methods for Initial-value Problems,* 2nd edn, Interscience, New-York.

Rogers, L. (1947) The Function of the Circulus Arteriosus of Willis. *Brain* **70,** 171–178.

Ruch, T. C. and Patton, M. D. (1974) *Physiology and Biophysics. Circulation, Respiration and Fluid Balance,* 20th edn. W. B. Saunders, Philadelphia.

Söderberg, U. and Weckmann, N. (1959) Changes in cerebral blood supply caused by changes in the pressure drop along arteries to the brain of the cat. *Experientia* **15,** 346–348.

Tuor, U. I. and Farrar, J. K. (1984) Pial vessel caliber and cerebral blood flow during hemorrhage and hypercapnia in the rabbit. *Am. J. Physiol.* **247,** H40–H51.

Van Der Eecken, H. M. (1959) Les anastomoses des artères leptominingées de l'encéphale et leur signification morphologique. *C. R. Ass. Anat.* **101,** 2–41.

Warming, R. F., Beam, R. M. and Yee, H. C. (1983). Stability of difference approximations for initial-boundary-value problems. *Proceedings of the Third International Symposium on Numerical Methods in Engineering* (Edited by Lascaus, P.), pp. 93–117, Paris.

Zagzoule, M. (1983) Circulation cérébrale: modélisation mathématique. Thesis. Université Paul Sabatier, Toulouse.